JOURNAL OF THERMOPHYSICS AND HEAT TRANSFER
Vol. 24, No. 1, January–March 2010

Freezing Front Propagation on Microgrooved Substrates

Yongfang Zhong*
Pennsylvania State University, Erie, Pennsylvania 16563
and
Anthony M. Jacobi† and John G. Georgiadis‡
University of Illinois at Urbana–Champaign, Urbana, Illinois 61801

DOI: 10.2514/1.46456

An experimental and numerical study of a planar freezing front propagating in a water layer above microgrooved substrates is presented. Classical photolithographic technology is employed to fabricate the microgrooves, and the morphological effect on the front propagation speed is quantified and compared with that predicted by the numerical simulation. The simulation is performed using enthalpy method and the finite element analysis package FIDAP in order to understand the physical mechanisms. The experimental results show that the speed of a freezing front oscillates when the front moves across the adjacent crests and troughs of microgrooves. The propagation speed on crests is about two to eight times that in troughs. The simulation results agree well with experiments and demonstrate that the silicon crests change the heat transfer direction into vertical as the latent heat is released from the freezing front, leading to a fast propagation on crests. The shape of the freezing front, the impact of the sample geometry, and the cooling rate of the system are also reported and discussed. The findings provide insight into how the speed and shape of a freezing front can be manipulated and might find broad application in systems with solidification.

Nomenclature

A	=	temperature at the cold end of a unit cell under the initial condition
B	=	temperature at the hot end of a unit cell under the initial condition
C_p	=	specific heat
d	=	depth of the trough
d_s	=	thickness of the substrate
d_w	=	water thickness above the substrate
H	=	enthalpy
$-K$	=	cooling rate derived from the curve fit of the experimental data
k	=	thermal conductivity
L	=	latent heat of water, 333.6 kJ/kg for water
$\tilde{n}_1$	=	normal direction of the freezing front (solid–liquid interface) in the water layer
$\tilde{n}_2$	=	normal direction of the silicon–water interface
T	=	temperature
T_f	=	melting temperature of ice, 0°C (273.2 K)
t	=	time
V	=	volume of water
w	=	width of the microgrooves
x	=	horizontal direction, i.e., the direction of the freezing front propagation
z	=	vertical direction
α	=	volumetric ratio of the water above a trough to the water above a crest
$\Delta T/\Delta x$	=	temperature gradient in the horizontal direction
Δt	=	time period calculated from the simulation
$\Delta\tau$	=	time period measured in the experiments
δ	=	Dirac delta function
ρ	=	density
v	=	speed
$v_{\tilde{n}_1}$	=	freezing front propagation speed, i.e., solidification rate
$\bar{v}_0$	=	speed of the water freezing point ($T = 0$°C) calculated from the simulation
ϕ	=	angle of the wedgelike front from the horizontal direction

Subscripts

c	=	cold end of the test specimen, or the crest of the microgrooves
f	=	freezing front, i.e., solid–liquid interface
h	=	hot end of the test specimen
s	=	silicon
t	=	trough of the microgrooves
w	=	water, including its liquid phase and solid phase
0	=	water freezing point ($T = 0$°C)

Superscripts

l	=	liquid phase of water
s	=	solid phase of water (ice)

I. Introduction

PROPAGATION of a freezing front can be found in many applications, such as crystal growth in casting [1,2], food processing [3], the purification of pollutants [4], cell cryopreservation [5,6], and cryosurgery [7,8]. The speed of a freezing front, i.e., the solidifying rate of the liquid–solid interface, is important to the time period required for a freezing process, the size of the crystal structures, and the interaction between the freezing front and the particles or cells. For example, the motion of the freezing front is directly related to the quality of casting [1,2]. The existence of critical solidifying rates determining the repellence or engulfment of particles or cells by a liquid–solid interface is widely recognized [4,5]. The front propagation speed on the order of 1 μm/s was found to provide the best pollutant reduction in the experiments [4]. The behavior of the particle-front interaction was also exploited to measure the surface tension of biological cells [6]. As a key factor in the outcome of cryotreatment, the solidifying rate of a freezing front

Received 23 July 2009; revision received 5 October 2009; accepted for publication 10 October 2009. Copyright © 2009 by the American Institute of Aeronautics and Astronautics, Inc. All rights reserved. Copies of this paper may be made for personal or internal use, on condition that the copier pay the $10.00 per-copy fee to the Copyright Clearance Center, Inc., 222 Rosewood Drive, Danvers, MA 01923; include the code 0887-8722/10 and $10.00 in correspondence with the CCC.

*Assistant Professor, School of Engineering, The Behrend College, 5101 Jordan Road.
†Professor, Department of Mechanical Science and Engineering, 1206 West Green Street.
‡Professor, Department of Mechanical Science and Engineering, 1206 West Green Street.

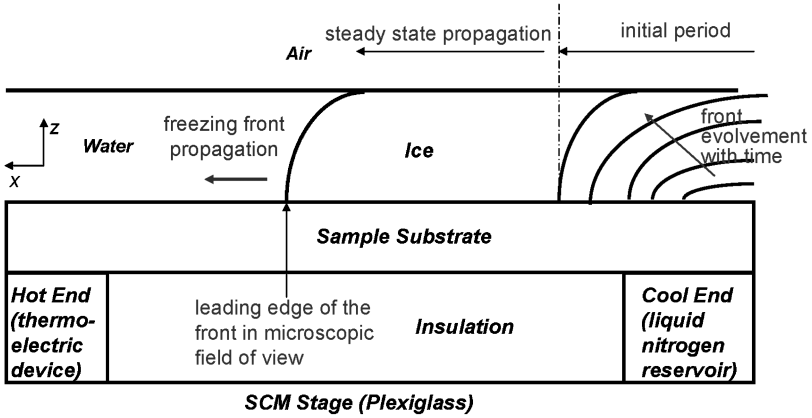

Fig. 1 Schematic of the vertical cross section of the test unit.

has attracted special attention in the development of cryosurgical devices [7,8]. Thus, knowledge of freezing front propagation is valuable, and the modification of its speed is useful in both traditional and interdisciplinary fields.

Many studies have investigated methods, such as thermal designs, for manipulating freezing front motion during its propagation. Zabaras et al. [2] and Xu and Naterer [9] provided useful numerical tools to obtain the required boundary flux and temperature conditions for a desired motion of the freezing front. Demirci et al. [10] applied a control method over heat fluxes and velocity of a freezing front to achieve specified casting properties and structures in materials processing. Hale et al. [11] proposed a general methodology to achieve independent management of the solidifying speed and the liquid-side interfacial temperature gradient. Stelian et al. [12] conducted a numerical study of a temperature oscillation effect on the freezing front speed in the vertical Bridgman growth process using the finite element analysis software FIDAP. Shu et al. [13] experimentally and numerically investigated the solid–liquid interface under the conditions of constant and oscillating temperature gradients, and their prediction was in good agreement with their experimental measurement. Furthermore, other effects (e.g., magnetic fields [14], capillary forces, and the solid–liquid contact angle [15]) on the solidifying interface have also been studied. With the photolithographic technology used in the integrated circuit (IC) industry, it has become economically feasible to fabricate microstructures on substrates to produce special performance effects in a wide range of systems [16–18]. However, the effect of these microstructures on the freezing front propagation has not been reported in the open literature, and there are reasons to believe it might have an important impact, as microstructure is known to be important in multiphase systems.

In this paper, an experimental and numerical study of a freezing front propagation in a thin water layer on microgrooved substrates is presented. Water is selected in the study because of its popularity and involvement in numerous applications. Microgrooves were fabricated on silicon substrates using photolithography, and an experimental apparatus was developed to produce a planar solid–liquid interface moving across the microgrooves. The repeatability achieved with the apparatus was verified, and careful experiments were performed to investigate the effect of microgrooves on the propagation speed of a freezing front. Quantitative results from the experiments were obtained and compared with the numerical simulation based on enthalpy method. The simulation was conducted using FIDAP, in order to help provide an understanding of the dominant mechanisms causing the behavior of the freezing front observed in the experiments. The experimental data reported here can contribute to the database used to validate and enhance computer models, and the knowledge developed in this study can be applied to gain valuable insight on controlling and modifying the speeds and shapes of a freezing front in engineering applications with solidification.

II. Experimental Method

A. Experimental Setup

An experimental apparatus was developed to generate a stable planar freezing front and to obtain the thermal data and the images of front propagation [19]. The vertical cross section of the test unit is schematically shown in Fig. 1, and the properties of materials used in the study are provided in Table 1. A layer of distilled water, enclosed by a rectangular glass frame, was deposited on the top of a silicon substrate. The substrate was fixed on two 9-mm-high copper blocks, which were spaced 22 mm apart and represented as the hot end and the cool end in Fig. 1. The substrate and the two ends were 38 mm long in the direction perpendicular to the vertical cross section and surrounded by insulation material. The entire section was placed on a Plexiglas stage (thermal conductivity of Plexiglas is 0.21 W/m-K) under a scanning confocal microscope (SCM). The motion of the freezing front was recorded using the SCM. The test section was well insulated and placed in an environment in which the variations of air temperature and relative humidity above the water layer were within 3°C and 4%, respectively, during the experiments.

A freezing front was produced and propagated in the water layer when a temperature gradient between the hot end and the cold end was established. The temperature of the hot end was controlled by a thermoelectric device, and the cooling of the cold end was provided by a liquid-nitrogen reservoir. The thermoelectric device had programmable control on its temperature in the range of −20 to 100°C. The thermoelectric device was operated under preset conditions, and the experiment was initiated by connecting the cold end to the nitrogen reservoir to generate the freezing front propagation. The motion of the leading edge of the front was captured by microscope, and the thermal conditions were simultaneously recorded. During the initial period of

Table 1 Properties of the materials

Material	Density ρ, kg/m^3	Thermal conductivity k, W/m-K	Specific heat C_p, J/kg-K	Thermal diffusivity $\alpha \times 10^6$, m^2/s
Water (Liquid)	1000	0.56	4200	0.14
Ice	920	1.89	2036	1.01
Silicon	2330	150	709	90
Air[a]	1.18	0.03	1007	22
Copper	8934	401	385	117

[a]Air is evaluated at 25°C and one atmospheric pressure.

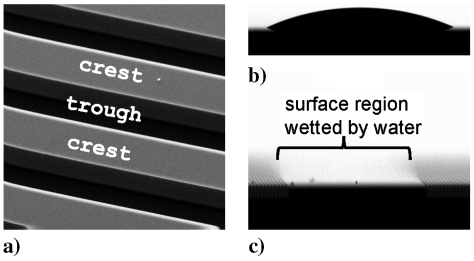

Fig. 2 Sample microstructure and the wetting behavior of water: a) SEM image of the microgrooved surface, viewed with an angle of 45° from horizontal direction, b) the images of a droplet on untreated flat silicon surface, and c) the image taken after droplets were deposited and penetrated into the microgrooved substrate.

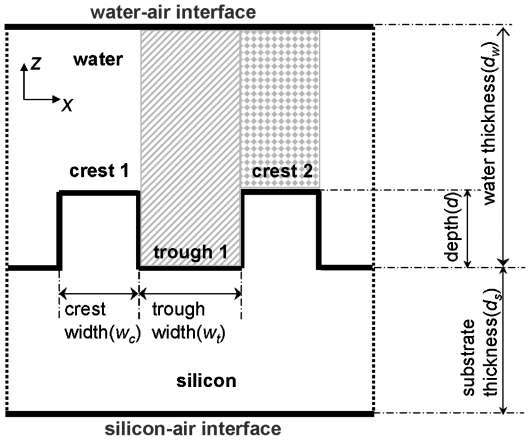

Fig. 3 A unit cell of the periodic microgrooved sample surface with a thin water layer.

the propagation, the front developed and moved at varying speeds. When the temperature of the hot and cold ends decreased at the same rate, resulting in a constant temperature difference between two ends, the freezing front propagated in the water layer at a constant speed. This period is called steady-state propagation in this study, and the motion of the freezing front during the steady-state propagation is investigated and reported in this paper.

B. Samples

Microgrooves were fabricated on silicon substrates using standard photolithographic methods in a class-100 clean room. Silicon wafers of test grade with a diameter of 4 in. and a thickness of 500 μm were used as sample substrates. Material removal from the substrate, the key step of the fabrication, was conducted using a PlasmaTherm Inductively Coupled Plasma-Deep Reactive Ion Etching (ICP-DRIE) system, which can produce vertical sidewalls for the etched grooves and provide high aspect ratios of groove depth to its width. (Detailed information about ICP-DRIE is reported by Yeom et al. in [20].) This method creates well-controlled geometry of the microstructures on silicon sample substrates. An image of the microgrooves, which was obtained using a scanning electron microscope (SEM) with an angle of 45° between the sample surface and the horizontal direction, is shown in Fig. 2a. In comparing Figs. 2a and 3, note that the dark region between two crests in Fig. 2a is a trough and the water layer was deposited on the substrate with periodic crests and troughs to form a test specimen.

The wetting behavior of water on the sample substrates was characterized using a Cam 200 optical contact angle meter, and the result is illustrated in Figs. 2b and 2c. When droplets of 22.0 ± 0.5 μL were placed onto the surfaces using a microsyringe, a contact angle of 24° was formed on flat silicon substrates before the fabrication, as shown in Fig. 2b. On the microgrooved substrates, the droplets formed a thin film and penetrated into the grooves instantly after the deposition, due to the capillary effect. Figure 2c is an image recorded after a droplet was deposited on the grooved substrate, and it shows that the contact angle of water on the substrate disappears after fabrication. This behavior is caused by the ion-etching in the ICP-DRIE process. This process significantly reduces the surface energy at the water–substrate interface, and, as a result, the contact angle of water on the substrate becomes near-zero. Ion-etching was also conducted after a rectangular glass frame was installed on the grooved substrates, in order to obtain a near-zero contact angle between the water–air interface and the top surface of the glass frame and to ensure the flatness of the water–air interface above the water layer.

The specifications of the test specimens are provided in Table 2, and the geometric parameters are defined in Fig. 3. In comparing Fig. 3 to Fig. 1, note that the configuration of the interface between the water layer and the substrates is simplified as a straight line in Fig. 1. Figure 3 illustrates the spatially periodic structure of the microgrooved substrates. The grooves are designed to have identical geometric parameters; two periodic structures, including two crests, one trough, and two half-troughs, are shown in Fig. 3 as a unit cell. The upper boundary and the bottom boundary of the unit cell are water–air interface and silicon–air interface, respectively. In addition to the geometric parameters shown in Fig. 3, the volumetric ratio of the water above a trough (the region with diagonal lines) to the water above a crest (the dotted region) is also listed in Table 2, for the discussion in the Results and Discussion section.

C. Measurement and Uncertainty

The geometric parameters of the test specimens shown in Fig. 3 were measured using a SCM. The SCM field of view was calibrated through imaging NIST—traceable 10 μm borosilicate microspheres with an uncertainty smaller than ± 0.7 μm in diameter. A minimum of 10 spheres were imaged and measured to determine the scale bar in the images obtained by the SCM. The geometry in the horizontal direction (the x direction in Fig. 3) was measured from the SCM images by comparing the distance with the scale bar. The geometry in the vertical direction (the z direction in Fig. 3) was measured by changing the focal plane of the SCM on different interfaces and recording its vertical position [19]. For each specimen, 10 locations were randomly selected to conduct the measurement, and an average value is reported. The measurements obtained from the SCM were compared with those from a contact profilometer, and the results from these two instruments were found to be within 1.0 μm. The uncertainty in the geometry of the test specimens shown in Table 2 is estimated to be ± 1 μm.

The propagation speed of the freezing front was determined from the images obtained by the SCM in the experiments. An example image of the front propagation is shown in Fig. 4. There are two distinct regions in this image: the bottom region, with adjacent bright and dark stripes, is the area with the microgrooves; and the upper,

Table 2 Specifications of the test specimens

Sample	Crest width w_c, μm	Trough depth d, μm	Trough width w_t, μm	Substrate thickness d_s, μm	Water thickness d_w, μm	Volumetric ratio α
1	299	33	301	467	433	1.090
2	297	112	303	388	512	1.306
3	298	95	302	405	495	1.254
4	259	246	341	254	446	2.936
5	244	290	356	210	490	3.575

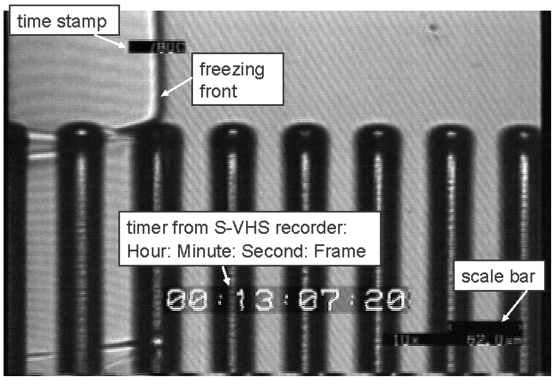

Fig. 4 An example image captured during the freezing front propagation experiments.

bright region is the untreated flat substrate. The bright stripes are the crests, and the dark ones are troughs of the grooves. In Fig. 4, the freezing front is the black line on the flat substrate in the upper region, and it is in the third trough (counted from the left) of the grooved area. Three symbols are imposed in each image: a time stamp at the upper left corner, a timer in the middle, and a scale bar at the bottom right corner. The time stamp is inputted by the LabVIEW program and indicates the elapsed time (in seconds) since the start of the experiment. This time stamp is consistent with the elapsed time used to simultaneously record the thermal conditions in the experiments. The timer in the middle of the image is added by the video recorder and indicates the hours, minutes, seconds, and frame number of the video images since the start of video recording. The scale bar provides the standard length for the movement of the freezing front. The average speed of the freezing front propagation on the crest and in the trough was obtained from the image sequence recorded in the experiments. The average velocity on the crest (or in the trough) is equal to the distance that the front travels across the crest (or the trough) divided by its traveling duration. The uncertainty in the movement of the front is estimated to be ± 2 μm, and the uncertainty in the period of front propagation is 0.015 s. The uncertainty in the average speed of front propagation [21] is within ± 1.0 μm/s.

To explore the relationship between the thermal conditions and the front propagation speed, the speed of the water freezing point moving on the silicon–air interface in Fig. 3 (i.e., the change of location on the bottom of the substrate where $T = 0$°C versus time) is obtained. Four thermocouples were installed on the air-side (bottom) surface of the sample substrate and separated at equal distances between the hot end and the cold end. During the steady-state propagation in the experiments, a linear temperature distribution was observed on the air-side surface of the sample substrate [19]. Hence, the position of the water freezing point was determined by a linear interpolation of the temperature measurements. The time period used to calculate the speed of the water freezing front is the same as that used to evaluate the freezing front speed. The time stamp at the upper left corner (shown in Fig. 4) is employed to identify the temperature profile corresponding to the front position and ensure that the calculated speeds of the front and the water freezing point are based on the same time. The uncertainty in propagation period is 0.5 s, and the uncertainty in temperature is 0.1°C. The uncertainty in the speed of the water freezing front [21] is estimated to be ± 0.5 μm/s. The experimental results are quantified and discussed in terms of the average front propagation speed on the crests and in the troughs, and of the average speed of the water freezing point on the air-side surface of the sample substrate.

III. Simulation

A simulation based on heat conduction in the water layer on the silicon substrate was developed to understand the propagation speed of the freezing front, because heat conduction plays an important role in the solidification of a thin layer [1]. The goal of this model is to explore whether the speed of the freezing front over crests and troughs is driven mainly by thermal effects or whether other factors might be important. It is aimed at identifying the important physical mechanisms, rather than providing an accurate prediction of experimental data. The calculation is carried out using the commercial software package FIDAP [22,23].

A. Problem Description

A unit cell, as shown in Fig. 3, was used as the spatial domain to solve the conduction problem due to the periodicity of the microgrooves on the substrate. Two materials, water and silicon, are contained in the unit cell, and the water layer contains both liquid phase and solid phase. The steady-state propagation, during which the temperature of the cold end and the hot end decreases at an identical rate, was considered. The experimental setup was tested, and the results showed that temperature variations in the direction perpendicular to the vertical cross section (shown in Fig. 3) were less than 0.3°C over the length of 30 mm (i.e., the thermocouples were installed over the distance of 30 mm in this test) on the air-side surface of the sample substrate. Hence, the problem was simulated as a two-dimensional, transient solidification problem with a moving solid–liquid interface in the water layer [19]. The mathematical description of this problem is given below, and the material properties used in the simulation are listed in Table 1.

In the solid phase of the water layer,

$$\rho_w^s C_{p,w}^s \frac{\partial T_w^s}{\partial t} = k_w^s \left(\frac{\partial^2 T_w^s}{\partial x^2} + \frac{\partial^2 T_w^s}{\partial z^2} \right) \tag{1}$$

In the liquid phase of the water layer,

$$\rho_w^l C_{p,w}^l \frac{\partial T_w^l}{\partial t} = k_w^l \left(\frac{\partial^2 T_w^l}{\partial x^2} + \frac{\partial^2 T_w^l}{\partial z^2} \right) \tag{2}$$

In the silicon,

$$\rho_s C_{p,s} \frac{\partial T_s}{\partial t} = k_s \left(\frac{\partial^2 T_s}{\partial x^2} + \frac{\partial^2 T_s}{\partial z^2} \right) \tag{3}$$

The conditions used to match the temperature and heat flux at the solid–liquid interface of the water are

$$k_w^s \frac{\partial T_w^s}{\partial \tilde{n}_1} - k_w^l \frac{\partial T_w^l}{\partial \tilde{n}_1} = \rho_w^s L v_{\tilde{n}_1} \tag{4}$$

$$T_w^s = T_w^l = T_f \tag{5}$$

Similar conditions of temperature and heat flux are applied at the silicon–water and silicon–ice interface to match the thermal condition between the two materials. These boundary conditions are

$$k_s \frac{\partial T_s}{\partial \tilde{n}_2} - k_w^s \frac{\partial T_w^s}{\partial \tilde{n}_2} = 0 \tag{6}$$

$$k_s \frac{\partial T_s}{\partial \tilde{n}_2} - k_w^l \frac{\partial T_w^l}{\partial \tilde{n}_2} = 0 \tag{7}$$

$$T_w^s = T_s \tag{8}$$

$$T_w^l = T_s \tag{9}$$

Moreover, thermal conditions are imposed on the outside boundary of the unit cell. The heat flux in the z direction (as shown in Fig. 3) into air at the water–air interface and the silicon–air interface is estimated to be less than 5% of the latent heat released during the front propagation [19]. Therefore, adiabatic conditions are good approximations and are applied to the top and bottom boundaries of the unit cell:

$$\frac{\partial T}{\partial z} = 0 \tag{10}$$

The temperature boundaries on the left and the right sides of the unit cell are derived from experimental data and expressed to vary linearly with time. As mentioned previously in the measurement section, a linear temperature distribution on the air-side surface of the sample substrate was observed during the front propagation. The cooling rate of the two ends is equal during the steady-state propagation. Hence, these boundary conditions on the unit cell are

$$T_c = A + K \cdot t \tag{11}$$

$$T_h = B + K \cdot t \tag{12}$$

where A, B, and K are constants obtained by curve-fitting to the temperature measurement on the sample surface. The temperature gradient $\Delta T/\Delta x = (B - A)/(2w_c + 2w_t)$ is equal to the temperature gradient over the whole sample substrate.

The initial condition in this problem is associated with the development of the freezing front. Because a freezing front is formed before it propagates at a constant speed, a steady-state temperature field with a solidification front in the water layer is used as the initial condition for the system described by Eqs. (1–12) without the time and time-derivative terms; this initial temperature field is the steady-state solution of the system, equivalent to those equations without the time and time-derivative terms.

The problem described above is difficult to solve analytically, because the source term in Eq. (4) is coupled to the temperature field through the propagation speed of the freezing front and because the location and the shape of the freezing front is to be solved as an unknown. Analytical solution to such phase-change problems is restricted to those with a simple geometry and simple boundary conditions (such as the one-dimensional Stefan problem) [1]. Therefore, a numerical solution was pursued.

B. Numerical Method to Solve the Conduction Model

The freezing front in this study moves along the x direction in the entire domain of interest. Therefore, an enthalpy method [23–25] with a fixed grid is applied to obtain the numerical solution to Eqs. (1–12). At the freezing front, the jump in heat flux is proportional to the latent heat, which corresponds to an isothermal change in the enthalpy for water at its freezing point. To handle the latent heat effect, the specific heat is modeled by

$$C_{p,w} = \frac{\mathrm{d}H}{\mathrm{d}T} = C_{p,w}(T) + L\delta(T - T_f) \tag{13}$$

This approach reduces the problem with solid and liquid regions to a single-region problem with rapidly varying properties at the freezing front. In this study, a numerical approximation for the specific heat $C_{p,w}$, based on temporal averaging [23,25], is employed to ensure the accuracy of enthalpy method. The change in enthalpy from the value at the previous time step and the change in temperature from the value at the previous time step are used to obtain $C_{p,w}$:

$$C_{p,w} = \frac{\mathrm{d}H/dt}{\mathrm{d}T/dt} \tag{14}$$

Thus, the specific heat at the integration points is evaluated from the temperatures at these points using

$$C_{p,w} = \frac{H(T_i) - H(T_{i-1})}{T_i - T_{i-1}} \tag{15}$$

where the subscripts refer to time-step number. This method always detects the passage of the solidification front at an integration point. The specific heat is evaluated directly from the enthalpy–temperature curve, which is specified as one of the properties in the simulation.

The FIDAP fluid dynamics analysis package (version 8.7, FLUENT, Inc.) is used to obtain the solution, in order to understand the behavior of the freezing front [19]. The finite element method is employed to generate the discretized equations for each node. The computational domain is meshed into nonuniform cells, with denser grid points near the interfaces. The mesh of 72×128 cells is employed, and further mesh refinement leads to the change in temperature within 0.05°C. The trapezoidal rule is used to discretize the temporal term in the system of equations. The time-step size is selected using a variable time-integration procedure incorporated in FIDAP [22,23] and is computed based on controlling the local truncation error to be below 1.0×10^{-3}. The successive substitution method is used to solve the equations at each time step, and convergence is achieved when the relative errors in the nodal values of the temperature and the relative errors in the residuals of the energy equations are both less than 0.01. The correct use of FIDAP codes is verified by comparing the numerical solutions of the one-dimensional Stefan problem with its analytical solutions.

IV. Results and Discussion

The speed of the freezing front is reported during the steady-state propagation when the temperatures of the cold end and hot end decrease at the same rate. Figure 5 provides representative results obtained from one experiment, and Table 3 summarizes the experimental results with different samples and conditions. As shown in Fig. 5, three speeds are quantified: v_c, the speed with which the front passes across one crest (as shown from point B to point C in the figure insert); v_t, the speed with which the front passes through one trough from point A to point B; and v_0, the speed of the water freezing point ($T = 0$°C) at the air-side surface of the substrate during the same period in which the front moves across the crest or

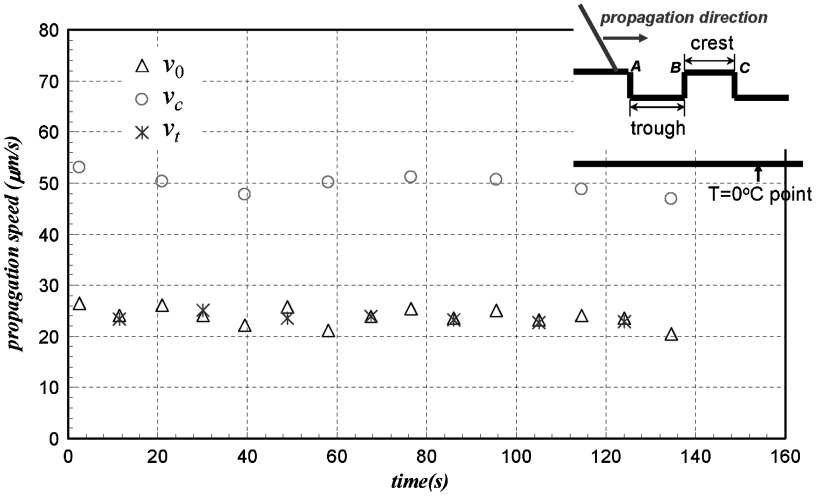

Fig. 5 Experimental data of the freezing front propagation (e.g., experiment no. 1).

Table 3 Summary of the propagation speeds observed in experiments

Exp. no.	v_0, μm/s	Sample no.	v_c, μm/s	v_t, μm/s	v_t/v_0	v_c/v_0	v_c/v_t
1	24.0	1	50.3	23.5	0.98	2.09	2.14
2	24.2	1	51.1	24.4	1.01	2.11	2.10
3	24.4	3	91.0	17.4	0.71	3.72	5.23
4	24.1	5	116.6	14.5	0.60	4.85	8.07
5	24.7	4	128.9	17.5	0.71	5.22	7.38
6	21.0	2	142.3	19.2	0.91	6.77	7.43
7	22.9	5	89.3	15.6	0.68	3.89	5.73
8	28.8	3	111.9	19.7	0.68	3.89	5.68

the trough. The data provided in Table 3 are the average speed as the front traveled across multiple crests and troughs on one sample; the data for every crest and trough of the substrate in each experiment (as shown in Fig. 5) are documented in [19].

Eight experiments are presented in this paper, in order to show the repeatability achieved with the experimental apparatus and the effect of surface microgrooves on the front propagation speed at various cooling rates. Because the motion of the freezing front is caused by the continuous temperature decrease of the cold end and the hot end, the movement of the water freezing point ($T = 0$°C) is an important measurement associated with the speed of the freezing front. Hence, the experiments were designed to allow control of the cooling rates of the cold and hot ends to provide different speeds of water freezing point v_0, as shown in the second column of Table 3. Experiments were first conducted with v_0 approximately 24.3 μm/s (ranging from 24.0 to 24.7 μm/s), and were then conducted with v_0 varying between 21.0 and 28.8 μm/s. Another controllable parameter in the experiments was the sample geometry, and different test specimens were used in the experiments, as shown in the third column of Table 3. Experiment nos. 1 and 2 are shown here as an example, in order to demonstrate the experimental repeatability, and the difference of the front propagation speed obtained from these two experiments is less than 1 μm/s and within the experimental uncertainty. The apparatus developed in this study is able to provide highly repeatable experimental results.

The experimental data show that the microgrooves on the silicon substrates significantly alter the speed of the freezing front in a thin water layer. First of all, the speed of a freezing front is observed to oscillate as the front propagates across adjacent crests and troughs. The propagation speed on the crests is two to eight times that of the speed in the troughs for the specimens used in these experiments. As shown in Fig. 5, the front propagation speed on a crest or in a trough is nearly constant when the water freezing point moves at a near-constant speed. In comparison to the movement of the water freezing point, the front moves at an equal or slightly slower speed in the trough, as shown in Table 3, where the value of v_t/v_0 is in the range of 0.68 to 1.01; the front propagates much faster on the crest, and the value of v_c/v_0 is more than 2.09 (the largest is 6.77 in experiment no. 6). Hence, the silicon microgrooves periodically modify the front speed when the front moves over a sequence of crests and troughs in the water layer.

The substrate geometry and the speed of the water freezing point v_0 have an impact on the change of the freezing front propagation speed. The ratio of v_c to v_t is strongly correlated to the volumetric ratio of the water above a trough to the water above a crest when the water freezing point propagates at an equal speed on different specimens. As given in Table 2 and illustrated in Fig. 3, the volumetric ratio of test specimens 1, 3, 4, and 5 is 1.090, 1.254, 2.936, and 3.575, respectively. The value of v_c/v_0 from the experiments with these specimens is 2.10, 5.23, 7.38, and 8.07, respectively, when the water freezing point moves at the average speed of 24.3 μm/s. This behavior indicates that the ratio of front speed on a crest to that in a trough increases with an increase in the water volumetric ratio. Furthermore, when v_0 increases in the experiments with the same test specimen (cf. experiment no. 7 to 4 and cf. experiment no. 3 to 8), the ratio of v_c to v_t increases, the ratio of v_c to v_0 increases, and the ratio of v_t to v_0 decreases.

To benefit engineering applications where front speed is critical, it is important to understand the mechanism causing the significant changes of the freezing front propagation speed over microgrooves observed in the experiments. The ratio of propagation speeds (v_c/v_0) is observed to be related to the volumetric ratio of water, as discussed above. Hence, one intuitive reason is that solidification takes more time in a trough than on a crest, simply because there is more water to be frozen above a trough than above a crest. To examine whether this simple explanation is viable as the sole cause of the difference, a wedgelike front (lines AA', BB', and CC', shown in Fig. 6) is assumed. If the large amount of water in a trough is the only reason for the decrease in the front propagation speed, then it is reasonable to assume that all other conditions remain the same in a trough and on a crest. Thus, the instantaneous solidification rate v is equal everywhere, and the shape of the front is repeatable on the periodic structure of the grooves. Under this assumption, the ratio of the front speed on a crest ($v_c = w_c/\Delta\tau_c = w_c v/(\rho V_c)$) to the front speed in a trough ($v_t = w_t/\Delta\tau_t = w_t v/(\rho V_t)$) can be reduced to $(w_c/w_t)(V_t/V_c)$. This ratio is equal to $\alpha(w_c/w_t)$, because the ratio of the water between lines AA' and BB' to the water between lines BB' and CC' is equal to the ratio of the water above a trough to the water above a crest. Based on the values of α, w_c, and w_t, given in Table 2, this assumption significantly underestimates the ratio of the front propagation speeds observed in the experiments. For example, the value of $\alpha(w_c/w_t)$ for sample no. 5 is 2.45, while the ratio of v_c to v_t, obtained from experiment no. 4, is 8.07. Therefore, the difference in water volume alone does not explain the difference in the speeds. The freezing front may take a complex shape, and the local solidifying speed may vary as the front propagates across the microgrooves.

The heat conduction model described earlier provides a better understanding of the change in the propagation speed and the shape of the freezing front. A comparison between the experimental data and simulation result is given in Table 4, with the dimensionless geometry of the test specimens given in Table 5. Because only the leading edge of the freezing front at the water–silicon interface is in the field of view of the SCM (as shown in Fig. 1) and recorded in the experiments, the point of $T = 0$°C at the water–silicon interface in the simulation is used to represent the leading edge, in order to make the simulation results consistent with experimental data. In Table 4, the time period required for the point of $T = 0$°C to move across the top edges of the

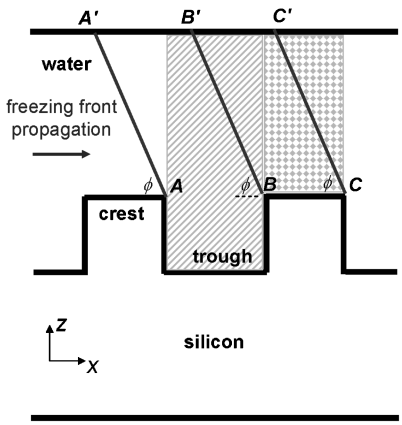

Fig. 6 Schematic of wedgelike freezing front associated with volumetric ratio of the frozen water.

Table 4 Comparison between experimental data and simulation results

	Experimental data				Simulation results				
Sample	Exp. no.	v_0, μm/s	$\Delta\tau_c$, s	$\Delta\tau_t$, s	$\Delta T/\Delta x$, °C/mm	$-K$, °C/s	$\bar{v}_0$, μm/s	Δt_c, s	Δt_t, s
3	3	24.4	3.2	17.4	2.6	0.074	27.1	3.7	16.6
3	8	28.8	2.7	15.3	2.7	0.086	31.5	3.1	14.3
2	6	21.0	2.1	15.8	2.5	0.053	19.5	4.0	24.0
5	7	22.9	2.7	22.8	2.5	0.040	16.1	0.4	37.0
5	4	24.1	2.1	24.6	2.6	0.060	24.1	0.4	24.6

Table 5 Dimensionless geometry of the test specimens

Sample	d_w, μm	w_c/d_w	d/d_w	w_t/d_w	$w_c/(d_w-d)$	$w_t/(d_w-d)$
2	512	0.58	0.22	0.59	0.74	0.59
3	495	0.60	0.19	0.61	0.74	0.61
5	490	0.50	0.59	0.73	1.22	0.73

grooves (as shown as points A, B, and C, in Fig. 5) is listed instead of the propagation speed, because the propagation distance in the simulation is set equal to that of the experiments, and thus the comparison is essentially conducted through the time period of the front propagation. In the simulation, $\Delta T/\Delta x$ and K are derived from experimental measurements, and $\bar{v}_0$, Δt_c, and Δt_t are calculated by the model. The simulation results show that $\bar{v}_0$, Δt_c, and Δt_t from the model reflect the same trends observed in the experiments. The model shows that the period for the front to cross a crest (Δt_c) is much smaller than to cross a trough (Δt_t), which is consistent with the experimental observation, i.e., $\Delta\tau_c \ll \Delta\tau_t$. This agreement between experimental data and the simulation results indicates that the thermal effect is the dominant mechanism for the speed oscillation of the freezing front across the microgrooves. Moreover, for samples nos. 2 and 3, Δt_c and Δt_t are of the same order of magnitude as $\Delta\tau_c$ and $\Delta\tau_t$, respectively, and the difference between $\bar{v}_0$ calculated from the model and v_0 measured in the experiments is smaller than 3.0 μm/s. For sample no. 5, Δt_c underestimates the experimental measurement $\Delta\tau_c$. This underestimation could be caused by geometric effects on the heat transfer and fluid flow in the water layer above the microgrooves [23]. As shown in Table 5, the difference between the dimensionless geometry of the samples nos. 2 and 3 is less than 5%, whereas sample no. 5 has a significantly different geometry. The effect of fluid flow resulting from sample geometry is not included in the heat-conduction model and thus cannot be captured by the current simulation.

Microconvection could exist in the liquid phase, especially in front of the moving freezing front [26–28]. Three forces might result in convection in the liquid phase: buoyancy-driven convection due to the effect of temperature variation on liquid density, surface-tension-driven convection due to the temperature variation at the water–air interface, and volume-change flow as a result of solidification. Because the ratio of the solid phase to the liquid phase is 0.92 and the solidification rate is small (in the order of tens of microns per second), the effect of volume-change flow is negligible [26]. Furthermore, the effect of buoyancy flow is also negligible, due to the small thickness of the liquid layer (in the order of 0.5 mm) [27]. Thus, thermocapillary flow due to surface tension is the only driven potential that could possibly result in convection in this study. In the case of thermocapillary flow, fluid is driven from hot to cold along the water–air interface by the surface tension gradient and recalculated as it approaches the freezing front. Turnover flow at the freezing front may convect heat, and the shape of the freezing front deviates from the one obtained from the heat-conduction model. For the conditions in this study, the Marangoni number is smaller than the critical Marangoni number for such convection to be important [19,29]. Nevertheless, numerical simulation with convection of heat taken into consideration might reduce the difference between experimental data and simulation results in this study. Additional experimental measurement on the liquid phase would be useful to evaluate the impact of heat convection in future study.

The isotherms obtained from the simulation are presented to provide further insight on the effect of microgrooves on the propagation speed and the shape of the front. The distribution of isotherms shows that the microgrooves significantly modify the temperature gradient in the region near the freezing front (isothermal line of $T = 0$°C) as the latent heat is released. Figures 7 and 8 illustrate the temperature distribution when the freezing front is in a trough or across a crest (see [19] for further detail). As shown in Figs. 7 and 8, the shape of the freezing front is wedgelike in the trough but has a thin filmlike leading edge on the crest. The filmlike leading edge is caused by the large temperature gradient in the z direction on the crest. Because the thermal diffusivity of silicon is approximately 600 times that of water and 90 times that of ice (the properties of the materials shown in Table 1), the silicon acts as a fin, and a large temperature gradient in the z direction is present near the crest. Hence, as compared with when the front is in a trough, the presence of a crest alters the isotherms and the direction of conduction is mostly in the z direction. The leading edge, which is observed in the experiments, is therefore found to cross the crest much faster than the front propagating through a trough. The microgrooves affect the temperature field and modify the shape and the propagation speed of the freezing front through a heat-conduction effect.

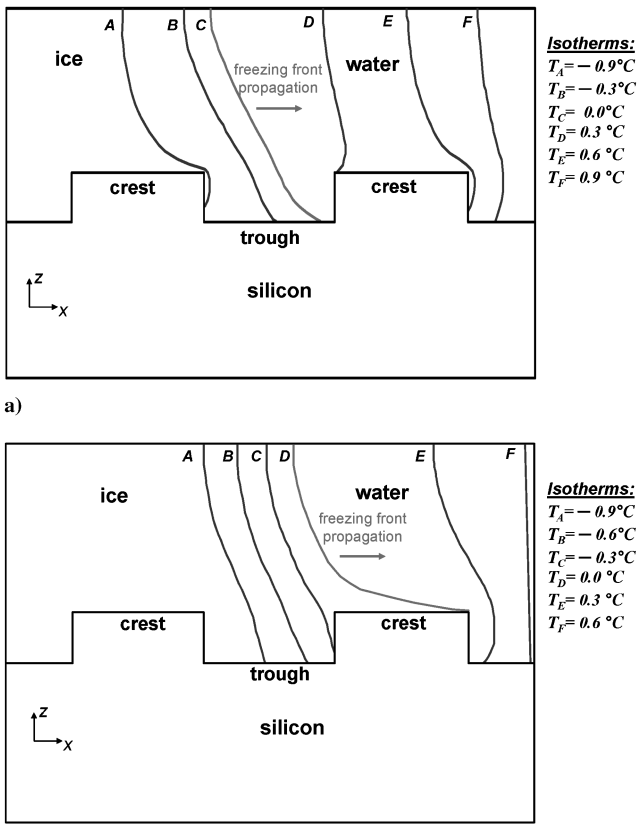

Fig. 7 Isotherms simulating experiment no. 6 (isothermal line of $T = 0$°C represents water–ice freezing front): a) the freezing front (line C) is in a trough, and b) the freezing front (line D) is on a crest.

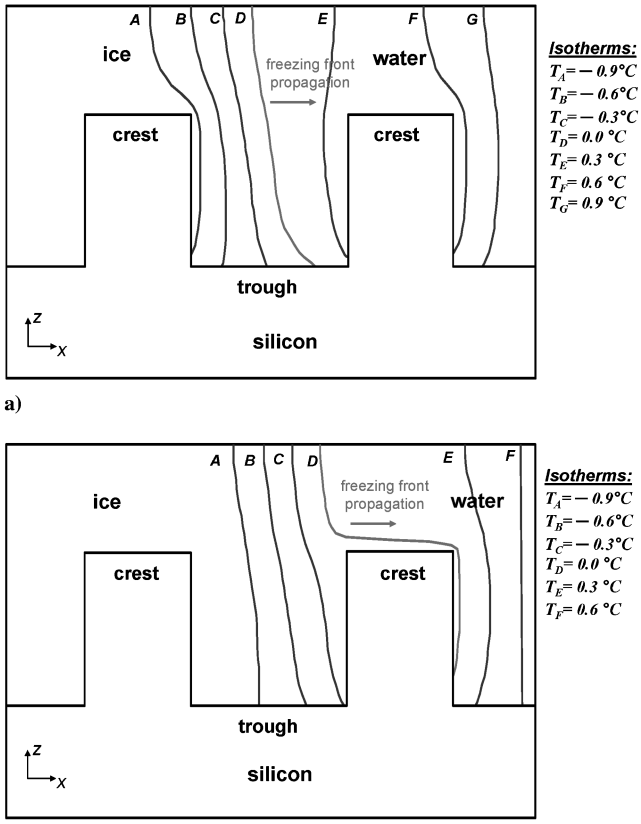

Fig. 8 Isotherms simulating experiment no. 4 (isothermal line of $T = 0°C$, line D, represents water–ice freezing front): a) the freezing front is in a trough, and b) the freezing front is on a crest.

The impact of the microgrooves on the shape of the freezing front due to the sample geometry is demonstrated qualitatively by comparison of Fig. 8 with Fig. 7. The shapes of the front in experiment nos. 3, 6, and 8 are alike due to the geometric similarity of the samples, and so are the front shapes in experiment nos. 4 and 7 [19]. With a substantial increase in the geometric parameters d/d_w and $w_c/(d_w - d)$, the area ratio of the crest to the entire domain of study increases. Comparing Fig. 7a with 8a, the slope of the freezing front increases and the latent heat is transferred mainly in the x direction for the case with the larger area ratio in Fig. 8a. On a crest, the freezing front is nearly parallel to the x direction, resulting from a small temperature gradient in the x direction and a large temperature gradient in the z direction. This gradient leads to a small period of time (as computed and listed as Δt_c in Table 4) for the point of $T = 0°C$ to move across the edges of the crest, and could result in a very thin layer of the solid phase uniformly covering the crest during this period for sample no. 5. Hence, the direction in which latent heat is transferred is altered when the area ratio of the silicon grooves increases: conduction in the z direction dominates on a crest, but in the x direction it dominates in a trough, due to the large thermal diffusivity of the grooves.

V. Conclusions

Freezing front propagation is important in a wide range of engineering applications, and advances in microfabrication open the possibility to manipulate the motion of the freezing front using microstructures. In this study, the focus was on freezing front propagation in a water layer above microgrooved substrates, with attention to the condition under which a constant temperature gradient is established and the water freezing point on the substrate moves at a nearly constant speed. Experimental data were obtained to investigate the effect of microgrooves on the speed of the freezing front propagation, and numerical simulation was performed to understand the behavior observed in the experiments.

The experimental results show that the propagation speed varies when the front moves across adjacent crests and troughs. The propagation speed on the crests is observed to be 2 to 8 times that in the troughs of the grooves. The ratio of the speed on the crests to that in the troughs increases with an increase in the volumetric ratio of the water above the trough to the water above the crest. However, the reason for the difference is more complicated than simply the amount of the water to be frozen in a trough. The simulation demonstrates that the microgrooves significantly modify the temperature gradient in the vicinity of the freezing front, as the latent heat is released in the troughs and on the crests. The results from the model are consistent with the experimental measurements, and the simulation predicts that the period for the front to cross a crest is much smaller than that required to cross a trough. The thermal effect (conduction in particular) is the dominant mechanism for the variations in the speed of the freezing front on the microgrooves. The heat conduction on a crest is mainly in the vertical direction, due to the large thermal diffusivity of silicon, and a much faster front propagation results. The shape of the freezing front, the impact of the sample geometry, and the cooling rate of the system are also reported and discussed.

Acknowledgments

Financial support of this work by the Air Conditioning and Refrigeration Center at the University of Illinois at Urbana–Champaign is gratefully acknowledged. The first author would like to thank Jonathan A. Dantzig of the University of Illinois for help with the simulation using FIDAP.

References

[1] Kurz, W., and Fisher, D. J., *Fundamentals of Solidification*, 3rd ed., Trans Tech Publications, Aedermannsdor, Switzerland, 1989, pp. 8–14.

[2] Zabaras, N., Ruan, Y., and Richmond, O., "Design of Two-Dimensional Stefan Processes with Desired Freezing Front Motions," *Numerical Heat Transfer*, Vol. 21, Part B, 1992, pp. 307–325. doi:10.1080/10407799208944907

[3] Navarro, A. S., Martino, M. N., and Zaritzky, N. E., "Effect of Freezing Rate on the Rheological Behavior of Systems Based on Starch and Lipid Phase," *Journal of Food Engineering*, Vol. 26, No. 4, 1995, pp. 481–495. doi:10.1016/0260-8774(94)00074-J

[4] Gay, G., and Azouni, A. M., "Forced Migration of Nonsoluble and Soluble Metallic Pollutants Ahead of a Liquid–Solid Interface During Unidirectional Freezing of Dilute Clayey Suspensions," *Crystal Growth and Design*, Vol. 2, No. 2, 2002, pp. 135–140. doi:10.1021/cg0100383

[5] Rubinsky, B., "Principles of Low Temperature Cell Preservation," *Heart Failure Reviews*, Vol. 8, No. 3, 2003, pp. 277–284. doi:10.1023/A:1024734003814

[6] Spelt, J. K., Absolom, D. R., Zingg, W., Van Oss, C. J., and Neumann, A. W., "Determination of the Surface Tension of Biological Cells Using the Freezing Front Technique," *Cell Biophysics*, Vol. 4, Nos. 2–3, 1982, pp. 117–131.

[7] Rabin, Y., Coleman, R., Mordohovch, D., Ber, R., and Shitzer, A., "A New Cryosurgical Device for Controlled Freezing 2. In Vivo Experiments on Skeletal Muscle of Rabbit Hindlimbs," *Cryobiology*, Vol. 33, No. 1, 1996, pp. 93–105. doi:10.1006/cryo.1996.0010

[8] Gage, A. A., Guest, K., Mantes, M., Caruana, J. A., and Whalen, D. A., Jr., "Effect of Varying Freezing and Thawing Rates in Experimental Cryosurgery," *Cryobiology*, Vol. 22, No. 2, 1985, pp. 175–182. doi:10.1016/0011-2240(85)90172-5

[9] Xu, R., and Naterer, G. F., "Controlling Phase Interface Motion in Inverse Heat Transfer Problems with Solidification," *Journal of Thermophysics and Heat Transfer*, Vol. 17, No. 4, Oct.–Dec. 2003, pp. 488–497. doi:10.2514/2.6808

[10] Demirci, H. H., Coulter, J. P., and Guceri, S. I., "A Numerical and Experimental Investigation of Neural Network-Based Intelligent Control of Molding Processes," *Journal of Manufacturing Science and Engineering*, Vol. 119, Feb. 1997, pp. 88–94. doi:10.1115/1.2836559

[11] Hale, S. W., Keyhani, M., and Frankel, J. I., "Design and Control of Interfacial Temperature Gradients in Solidification," *International Journal of Heat and Mass Transfer*, Vol. 43, No. 20, 2000, pp. 3795–3810.

doi:10.1016/S0017-9310(00)00011-9

[12] Stelian, C., Duffar, T., Santailler, J. L., and Nicoara, I., "Influence of Temperature Oscillation on the Interface Velocity During Bridgman Crystal Growth," *Journal of Crystal Growth*, Vols. 237–239, Nos. 1–4, 2002, pp. 1701–1706.
doi:10.1016/S0022-0248(01)02335-1

[13] Shu, Y., Li, B. Q., and de Groh, H. C., III, "Convection and Solidification in Constant and Oscillating Thermal Gradients: Measurements and Solidifications," *Journal of Thermophysics and Heat Transfer*, Vol. 19, No. 2, April–June 2005, pp. 199–208.
doi:10.2514/1.8809

[14] Li, K., Li, B. Q., and de Groh, H. C., "Three-Dimensional Gravity-Jitter Induced Melt Flow and Solidification in Magnetic Fields," *Journal of Thermophysics and Heat Transfer*, Vol. 17, No. 4, Oct.–Dec. 2003, pp. 498–508.
doi:10.2514/2.6795

[15] Sulfredge, C. D., Tagavi, K. A., and Chow, L. C., "Void Profiles in Unidirectional Solidification: The Role of Capillary Forces and Gravity," *Journal of Thermophysics and Heat Transfer*, Vol. 8, No. 3, July–Sept. 1994, pp. 608–617.
doi:10.2514/3.585

[16] Yoshimitsu, Z., and Nakajima, A., "Effects of Surface Structure on the Hydrophobicity and Sliding Behavior of Water Droplets," *Langmuir*, Vol. 18, No. 15, 2002, pp. 5818–5822.
doi:10.1021/la020088p

[17] Narhe, R. D., and Beysens, D. A., "Nucleation and Growth on a Superhydrophobic Grooved Surface," *Physical Review Letters*, Vol. 93, No. 7, 2004, Paper 076103.
doi:10.1103/PhysRevLett.93.076103

[18] Li, X. M., Reinhoudt, D., and Crego-Calama, M., "What Do We Need for a Superhydrophobic Surface? A Review on the Recent Progress in the Preparation of Superhydrophobic Surfaces," *Chemical Society Reviews*, Vol. 36, No. 8, 2007, pp. 1350–1368.
doi:10.1039/b602486f

[19] Zhong, Y., Jacobi, A. M., and Georgiadis, J. G., "Condensation and Freezing Front Propagation on Surfaces with Topographic and Chemical Modifications," Air Conditioning and Refrigeration Center TR-262, Urbana, IL, 2008.

[20] Yeom, J., Wu, Y., Selby, J. C., and Shannon, M. A., "Maximum Achievable Aspect Ratio in Deep Reactive Ion Etching of Silicon due to Aspect Ratio Dependent Transport and the Microloading Effect," *Journal of Vacuum Science and Technology B (Microelectronics and Nanometer Structures)*, Vol. 23, No. 6, 2005, pp. 2319–2329.
doi:10.1116/1.2101678

[21] Taylor, B. N., and Kuyatt, C. E., "Guidelines for Evaluating and Expressing the Uncertainty of NIST Measurement Results," National Inst. of Standards and Technology, TN 1297, Gaithersburg, MD, 1994.

[22] FIDAP, Fluid Dynamics Analysis Software Package, Ver. 8.7, FLUENT, Inc., Lebanon, NH, 2002.

[23] Dantzig, J. A., "Modelling Liquid–Solid Phase Changes with Melt Convection," *International Journal for Numerical Methods in Engineering*, Vol. 28, No. 8, 1989, pp. 1769–1785.
doi:10.1002/nme.1620280805

[24] Voller, V. R., and Cross, M., "Accurate Solutions of Moving Boundary Problems Using the Enthalpy Method," *International Journal of Heat and Mass Transfer*, Vol. 24, No. 3, 1981, pp. 545–556.
doi:10.1016/0017-9310(81)90062-4

[25] Voller, V. R., Swaminathan, C. R., and Thomas, B. G., "Fixed Grid Technique for Phase Change Problems: A Review," *International Journal for Numerical Methods in Engineering*, Vol. 30, No. 4, 1990, pp. 875–898.
doi:10.1002/nme.1620300419

[26] Anderson, A. M., and Davis, S. H., "Solidification of Free Liquid Films," *Journal of Fluid Mechanics*, Vol. 617, Dec. 2008, pp. 87–106.
doi:10.1017/S0022112008003753

[27] Kirdyashkin, A. G., "Thermogravitational and Thermocapillary Flows in a Horizontal Liquid Layer Under the Conditions of a Horizontal Temperature Gradient," *International Journal of Heat and Mass Transfer*, Vol. 27, No. 8, 1984, pp. 1205–1218.
doi:10.1016/0017-9310(84)90048-6

[28] Villers, D., and Platten, J. K., "Coupled Buoyancy and Marangoni Convection in Acetone: Experiments and Comparison with Numerical Simulations," *Journal of Fluid Mechanics*, Vol. 234, Jan. 1992, pp. 487–510.
doi:10.1017/S0022112092000880

[29] Carey, V. P., *Liquid-Vapor Phase-Change Phenomena: An Introduction to the Thermophysics of Vaporization and Condensation Processes in Heat Transfer Equipment*, Taylor and Francis, London, 1992, pp. 46–51.